



**HAL**  
open science

## Beyond $\gamma$ -Al<sub>2</sub>O<sub>3</sub> crystallite surfaces: The hidden features of edges revealed by solid-state <sup>1</sup>H NMR and DFT calculations

Ana T.F. Batista, Dorothea Wisser, Thomas Pigeon, David Gajan, Fabrice Diehl, Mickael Rivallan, Leonor Catita, Anne-Sophie Gay, Anne Lesage, Céline Chizallet, et al.

### ► To cite this version:

Ana T.F. Batista, Dorothea Wisser, Thomas Pigeon, David Gajan, Fabrice Diehl, et al.. Beyond  $\gamma$ -Al<sub>2</sub>O<sub>3</sub> crystallite surfaces: The hidden features of edges revealed by solid-state <sup>1</sup>H NMR and DFT calculations. *Journal of Catalysis*, 2019, 378, pp.140-143. 10.1016/j.jcat.2019.08.009 . hal-02333915

**HAL Id: hal-02333915**

**<https://ifp.hal.science/hal-02333915>**

Submitted on 29 Oct 2019

**HAL** is a multi-disciplinary open access archive for the deposit and dissemination of scientific research documents, whether they are published or not. The documents may come from teaching and research institutions in France or abroad, or from public or private research centers.

L'archive ouverte pluridisciplinaire **HAL**, est destinée au dépôt et à la diffusion de documents scientifiques de niveau recherche, publiés ou non, émanant des établissements d'enseignement et de recherche français ou étrangers, des laboratoires publics ou privés.

1 **Beyond  $\gamma$ -Al<sub>2</sub>O<sub>3</sub> Crystallite Surfaces: the Hidden Features of Edges Revealed by Solid-**  
2 **State <sup>1</sup>H NMR and DFT Calculations**

3 Ana T. F. Batista <sup>a</sup>, Dorothea Wisser <sup>a,b</sup>, Thomas Pigeon <sup>a</sup>, David Gajan <sup>b</sup>, Fabrice Diehl <sup>a</sup>,  
4 Mickael Rivallan <sup>a</sup>, Leonor Catita <sup>a</sup>, Anne-Sophie Gay <sup>a</sup>, Anne Lesage <sup>b</sup>, Céline Chizallet <sup>a</sup>, and  
5 Pascal Raybaud <sup>a,\*</sup>

6 <sup>a</sup> IFP Energies nouvelles, Rond-point de l'échangeur de Solaize, 69360 Solaize (France)

7 <sup>b</sup> Centre de RMN À Très Hauts Champs, Université de Lyon (CNRS/ENS Lyon/UCB Lyon  
8 1), 69100 Villeurbanne (France)

9 Corresponding author: Pascal Raybaud, E-mail address: [pascal.raybaud@ifpen.fr](mailto:pascal.raybaud@ifpen.fr)

10

11 **Abstract**

12 Elucidating the nature of high surface area gamma alumina sites is of great interest for  
13 numerous applications. In this work, the structural and spectroscopic features of edge sites are  
14 unravelled thanks to density functional theory (DFT) calculations combined with high field  
15 <sup>1</sup>H MAS NMR of two high surface area alumina samples of distinct morphologies. DFT  
16 chemical shift calculations were carried out for relevant surface models with different  
17 hydration degrees. However, the best assignment is achieved by considering the first DFT  
18 model representing the hydroxylated edges located at the intersection of (110) and (100)  
19 alumina facets. The sharp <sup>1</sup>H NMR peak at 0 ppm corresponds to  $\mu_1$ -OH groups which are  
20 located on this edge and are free from hydrogen bonding. Moreover, we show that these edge  
21 sites are the most reactive with respect to chlorine exchange.

22

23 **Keywords:** alumina, density functional theory, edge, hydroxyls, NMR spectroscopy

24

25

## 26 **1. Introduction**

27 The gamma polymorph of  $\text{Al}_2\text{O}_3$  is used in numerous industrial applications thanks to its  
28 remarkable catalytic and adsorptive properties[1] which have been extensively studied by  
29 experimental and theoretical approaches.[2–9] In particular, surface hydroxyl groups,  
30 responsible for Brønsted acidity, have been characterized by infra-red (IR) spectroscopy  
31 [2,3,10–12] and by  $^1\text{H}$  solid-state nuclear magnetic resonance (NMR) spectroscopy.[12–16]  
32 Moreover, DFT calculations[5] enabled the refinement of the empirical assignment of the  
33 main IR bands thanks to the determination of the hydration of the three main exposed  $\gamma\text{-Al}_2\text{O}_3$   
34 surfaces:[17] (110), (100) and (111). In  $^1\text{H}$  NMR work, the use of high fields and fast magic  
35 angle spinning (MAS) provided improved spectral resolution, revealing various, partially  
36 resolved,  $^1\text{H}$  signals. Three main spectral regions were identified at around 0 ppm, 1-3 ppm  
37 and 3-5 ppm, respectively assigned to non H-bonded  $\mu_1\text{-OH}$ ;  $\mu_2\text{-OH}$  and  $\mu_3\text{-OH}$ . These  
38 hydroxyls are connected to one, two or three Al atoms exhibiting different coordination  
39 ( $\text{Al}_{\text{IV}}$ ,  $\text{Al}_{\text{IV}}$ ,  $\text{Al}_{\text{VI}}$ ).[15,16] Also, broad signals above 5 ppm were associated with hydrogen  
40 bond donor species.[16]

41 However, to go beyond the current knowledge of high surface aluminas, atomic scale insights  
42 into the nature and location of the hydroxyls that originate each signal are required. In  
43 particular, considering extended surfaces only to interpret NMR data overlooks that  $\gamma\text{-Al}_2\text{O}_3$   
44 crystallites are finite nano-objects exhibiting various morphologies. Like metallic nano-  
45 particles with stepped surfaces and edges that provide low coordination sites active in  
46 catalysis,[18–21] edge architectures present on alumina crystallites should harbour original  
47 hydroxyl and Al sites distinct from those on such surfaces. In a recent review, Busca points to  
48 the likely role of edges and corners on alumina's reactivity, which are suspected to be the  
49 location of the strongest Lewis acid sites bearing hydroxyl groups more resistant to  
50 dehydration.[8,22]

51 Here, the interpretation of the proton NMR spectra of  $\gamma$ -Al<sub>2</sub>O<sub>3</sub> is revisited, providing new  
52 insights into the nature and location of the hydroxyls in order to refine our current structural  
53 knowledge of high surface area aluminas. <sup>1</sup>H NMR spectra was recorded on two Al<sub>2</sub>O<sub>3</sub>  
54 samples of different morphologies, and it is shown by chemical shift DFT calculations that  
55 considering alumina facets only leads to an incomplete description of the spectra. This  
56 challenge is solved by establishing edge models highlighting the selective chlorination of the  
57 edge sites.

58

## 59 **2. Materials and methods**

60 Two relevant commercial high surface alumina samples are considered, PuralSB3 and TH100  
61 (Sasol), labelled *P-egg* and *T-flat* respectively, exhibiting different high BET surfaces  
62 (S.I.S1). Their characterization by high-resolution transmission electron microscopy (HR-  
63 TEM) suggests that T-flat crystallites are larger and have a better defined and more  
64 parallelepipedic platelet-like morphology than P-egg's, which appear to have a round shape  
65 (S.I.S1). Chlorinated alumina samples were prepared by exposing alumina to a HCl solution  
66 (3.5%<sub>w</sub>Cl/g<sub>dry alumina</sub>) for 45 minutes, followed by drying and calcination at 520°C. After  
67 thermal treatment under H<sub>2</sub> for 2h at 500°C (ramp 5°C/min) and rotor packing under inert  
68 atmosphere, quantitative solid-state <sup>1</sup>H NMR spectra were acquired. H SS MAS NMR spectra  
69 were obtained on a SB Bruker Avance III 800 (800 MHz <sup>1</sup>H resonance frequency, 18.8 T)  
70 spectrometer using a zirconia 2.5 mm rotor at 30 kHz MAS. Quantitative <sup>1</sup>H spectra were  
71 recorded using a DEPTH[23–25] sequence for probe background suppression. Pre-scan delays  
72 were set to five times the <sup>1</sup>H longitudinal relaxation time (T<sub>1</sub>). Chemical shifts were  
73 referenced relative to adamantane. Spectral deconvolution was done using DMFit[26]. These  
74 spectra recorded at high magnetic field and relatively fast MAS reveal the surface OH signals  
75 and subtle changes in chemical shifts between the two different types of alumina (Figure 1 a).

76 To help for the interpretation of NMR experiments, chemical shifts (S.I.S2.3.) have been  
77 calculated by using the linear response approach[27,28] within the PBE-dDsC exchange  
78 correlation functional[29,30] and PAW pseudopotentials[31] with an energy cut off of 400 eV  
79 as implemented in the VASP code.[32,33] The average of the isotropic chemical shielding ( $\sigma$ )  
80 of each proton on a TMS (tetramethylsilane) model (a single molecule surrounded by  
81 vacuum) was used as reference to calculate the isotropic chemical shift ( $\delta$ ) of the protons of  
82 the various hydroxyls of the alumina surfaces or at the edges :

$$83 \quad \delta_{\text{iso}} = \sigma_{\text{iso}} - \sigma_{\text{ref}} \quad (1)$$

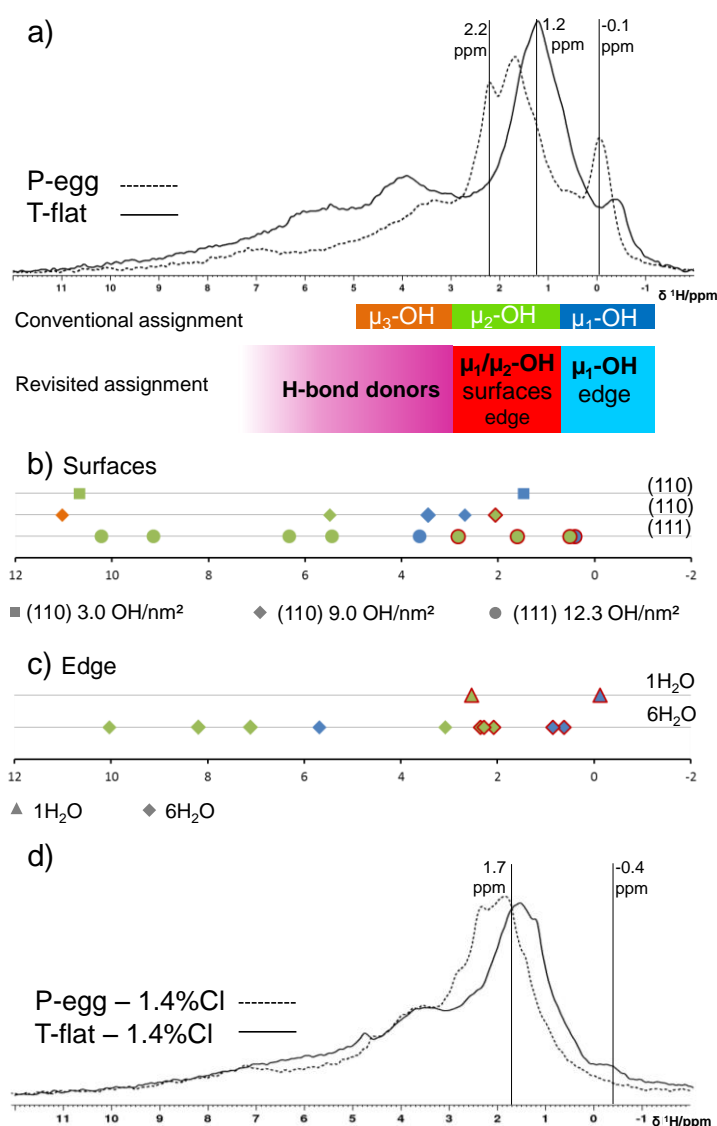
84 For that purpose, relevant periodic models of alumina (110), (100) and (111) surfaces and  
85 (110)-(100) edges have been constructed and optimized for various thermodynamically  
86 relevant hydration coverages depending on the experimental (T, P) analytical conditions  
87 (S.I.S2.). Geometry optimizations were performed using a conjugate-gradient algorithm and  
88 convergence criterion on forces of 0.01 eV Å<sup>-1</sup>.

89

### 90 **3. Results and Discussion**

91 <sup>1</sup>H NMR spectra of P-egg and of T-flat (Figure 1 a) present the main features expected for  $\gamma$ -  
92 Al<sub>2</sub>O<sub>3</sub>: a resolved signal at around 0 ppm; intense and well-defined peaks in the 1-3 ppm  
93 range and broad components ranging from 3-7 ppm. Moreover, the spectra of the two  
94 aluminas are clearly distinguished. The most remarkable difference is that the higher-field  
95 signal (at respectively -0.1 and -0.4 ppm) is much more intense for P-egg than for T-flat (12%  
96 vs 4% of total <sup>1</sup>H signal from spectral deconvolution, Table S2). The 1-3 ppm region is also  
97 distinguishable: for P-egg two main signals (1.6 and 2.2 ppm) are observed while for T-flat  
98 only one is (1.2 ppm), albeit some shoulders indicating other contributions. Lastly, the  
99 contribution of the broad signals ranging from 3-7 ppm is significantly more intense in the T-  
100 flat spectrum.

101 In order to rationalize these experimental results, chemical shifts were calculated (Figure 1 b  
 102 and S.I.S2.3) for hydrated surface models of the three main exposed  $\gamma$ -Al<sub>2</sub>O<sub>3</sub> surfaces[17]  
 103 (110), (100) and (111) as defined in previous DFT works [4,5,7] For each surface, several  
 104 hydration degrees were considered (S.I.S2.1.) in order to well represent the alumina samples  
 105 after thermal treatment, (Figure S8). In the experimental conditions,  $10^{-4} < P(\text{H}_2\text{O}) < 10^{-6}$  bar  
 106 and  $700\text{K} < T < 800\text{K}$ , the (110) surface exhibits 3.0 OH/nm<sup>2</sup> and 9.0 OH/nm<sup>2</sup>, the (111)  
 107 surface 12.3 OH/nm<sup>2</sup>, while the (100) surface is dehydrated.



108  
 109 **Figure 1.** a) <sup>1</sup>H MAS NMR spectra of two aluminas with different morphologies, P-egg and  
 110 T-flat (800 MHz, 30 kHz MAS). The conventional assignment and the revisited one are

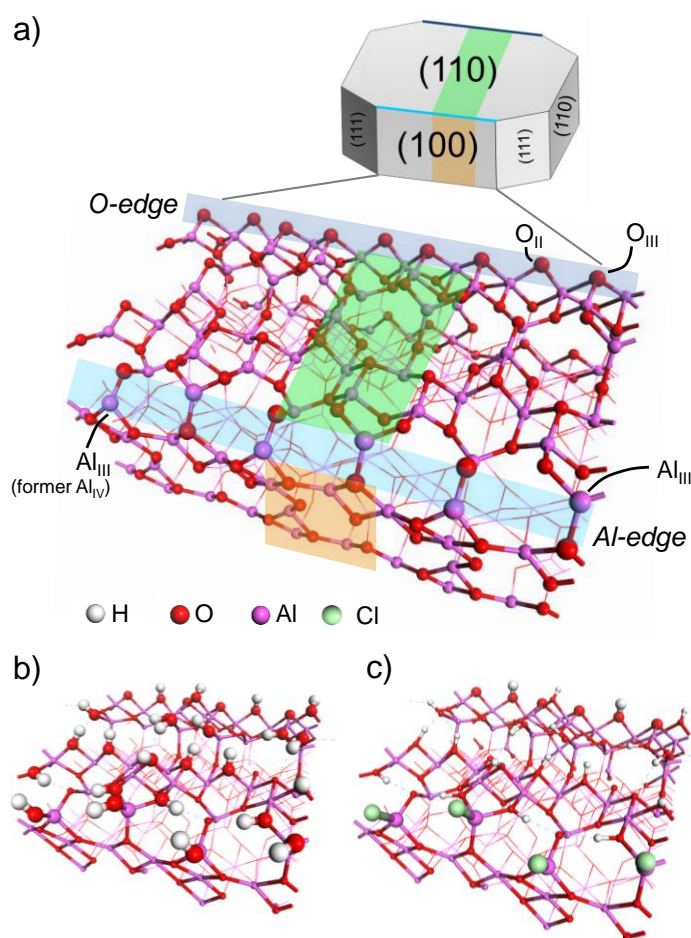
111 represented below. b)  $^1\text{H}$  chemical shifts calculated by DFT for hydroxyls, colour coded  
112 according to the type of OH group given in the conventional assignment, for three surface  
113 models; non H-bond donor hydroxyls are highlighted by red outlining. c)  $^1\text{H}$  chemical shifts  
114 calculated by DFT for hydroxyls for the (110)-(100) edge model at two hydration degrees. d)  
115  $^1\text{H}$  MAS NMR spectra (800 MHz, 30 kHz MAS) of chlorinated samples.

116  
117 First, it can be noted that most of the hydroxyls on these surfaces are involved in hydrogen  
118 bonding (Tables S8, S9, S10). Almost half of them are H-bond donors, resulting in high  
119 chemical shifts: several  $\mu_2$ -OH appearing at  $>5$  ppm. In this case, the chemical shift correlates  
120 with hydrogen bond length (Figures S11 and S12),[16,34–36] leading to large variations in  $\delta$ .  
121 Experimentally, H-bond donors are not expected to provide well defined signals such as the  
122 ones observed up to 3 ppm.[36]

123 Thus, we observe a poor correspondence between the previously proposed range and the  
124 simulated  $^1\text{H}$  chemical shifts which do not explain the below 0 ppm signal, expected to  
125 correspond to  $\mu_1$ -OH.[14,15] Contributions calculated at 0.4 and 0.8 ppm from  $\mu_1$ -OH and  $\mu_2$ -  
126 OH (respectively) of the (111) surface are found, while the classical assignment does not  
127 expect  $\mu_2$ -OH in this range. In addition, no  $\mu_3$ -OH are predicted in the 3-5 ppm region.  
128 Overall, these results show that the resonances observed in the experimental  $^1\text{H}$  NMR spectra  
129 of these  $\gamma$ - $\text{Al}_2\text{O}_3$  samples cannot be fully interpreted by considering only their crystalline  
130 surfaces. This trend holds true for any hydration degrees (S2.1 and S2.3).

131 To go beyond, another site architecture must be conceived. Apart from the empirical model  
132 proposed by Busca,[8] no atomistic model of alumina edge was previously reported in the  
133 literature. Thus, a novel model for the (110)-(100) edge was determined (Figure 2 a) based on  
134 a nano-rod structure (S.I.S2.2) resulting from the cleavage of the alumina bulk[37] in the two  
135 directions perpendicular to the (110) and (100) surfaces. This induces two edge-terminations,

136 one exposing Al atoms (here called Al-edge) and the other exposing O atoms (O-edge). The  
 137 Al-edge is constituted of one upper row of Al<sub>III</sub> atoms (also three-fold coordinated on the  
 138 (110) surface) and one lower row of Al<sub>III</sub> atoms that correspond to Al<sub>IV</sub> on the (110) surface.  
 139 The O-edge exhibits a row of alternating O<sub>II</sub> and O<sub>III</sub>, both formally O<sub>III</sub> on the (110) surface.  
 140 These rows of atoms on both edges will be referenced to as edge sites.  
 141



142  
 143 **Figure 2.** a) Alumina platelet scheme[5] and dehydrated edge model corresponding to two  
 144 possible edge terminations (blue) between the (110) (green, top) and the (100) (orange, sides)  
 145 surfaces. Edge sites are depicted by bigger balls. b) hydrated edge model with 6H<sub>2</sub>O and c)  
 146 chlorinated edge model constructed from the 6H<sub>2</sub>O hydrated model by exchanging Al-side μ<sub>1</sub>-  
 147 OH. Blue traced lines indicate hydrogen-bonds (bond length's threshold of 2.5 Å).  
 148

149 The systematic study of the hydration state of the nano-rod (and the corresponding edges)  
150 shows that water is the most strongly stabilized at the edge sites, rather than on the facet sites.  
151 For the adsorption of the first water molecule per unit cell of simulation, this leads to the  
152 formation of one  $\mu_2$ -OH, the  $H^+$  bonding to the  $O_{II}$  atom on the O-edge, and of one  $\mu_1$ -OH, the  
153  $OH^-$  bonding to the  $Al_{III}$  on the lower row on the Al-edge that relaxes into a tetragonal  
154 geometry (Table S7). Both these hydroxyls are not involved in hydrogen bonding. The  
155 corresponding adsorption energy is  $-436 \text{ kJ}\cdot\text{mol}^{-1}$ , which is far greater than usual adsorption  
156 energies reported on the alumina surfaces,[4] and is consistent with the chemical intuition that  
157 the reactivity of Lewis Al edge sites should be greater.[8] Such a configuration is a priori  
158 striking when thinking in terms of water dissociation, because the hydroxyl and the  
159 corresponding proton are not lying on the same kind of edge. However, one shall consider that  
160 experimentally, such low hydration states are obtained upon dehydration of the surface sites,  
161 making it possible to leave at the surface distant OH and H groups in the end, after  
162 recombination of other OH and H pairs. When more than two water molecules are adsorbed  
163 per unit cell of simulation, all the “edge sites” are saturated and the near edge sites on the  
164 (110) top surface of the nano-rod start being occupied (Figure 2 b), while the (100) facet of  
165 the rod remains dehydrated. These “near edge” sites exhibit a H-bond network identical to  
166 that of the surface models. In the conditions of thermal treatment ( $10^{-4} < P(H_2O) < 10^{-6}$  bar and  
167  $700\text{K} < T < 800\text{K}$ ), among the multiple hydration degrees equally stable (S.I. Figure S10), we  
168 choose two relevant cases: one and six adsorbed water molecules per pair of edges.  
169 The calculated  $^1H$  chemical shifts for the (110)-(100) edge with one and six adsorbed water  
170 molecules are represented in Figure 1 c).  $\mu_1$  and  $\mu_2$  hydroxyls on edge sites appear in the  
171 expected  $\delta$  range:  $\approx 0$  ppm and  $\approx 2$  ppm respectively. These OH are not only free from  
172 hydrogen bonding, but also isolated from other neighbouring hydroxyls. For 6  $H_2O$

173 molecules, hydroxyls with  $\delta > 3$  ppm are located on near edge sites and are H-bond donors, as  
174 the red outlining indicates.

175 With this edge model a significantly improved correlation between experimental and  
176 calculated chemical shifts is achieved, especially for the sharp peak at  $\approx 0$  ppm. Thus, this  
177 peak corresponds mostly to isolated  $\mu_1$ -OH located on the edges of alumina crystallites, which  
178 are free from hydrogen bonding. While the contribution of some free and H-bond acceptor  
179 species on the (111) surface cannot be ruled out, their contribution to the signal is minor, as  
180 discussed ahead. The 1-3 ppm region is expected to result from non-isolated  $\mu_1$ -OH and  $\mu_2$ -  
181 OH that are free from H-bonds or H-bond acceptors located on the edges and on the surfaces  
182 of the crystallites. The fact that in average, the  $\mu_2$ -OH sites are much more represented in this  
183 region with respect to the 0-1 ppm region, is in agreement with  $^1\text{H}$ - $^{27}\text{Al}$  RESPDOR  
184 experiments by Taoufik et al..[15] While not much insight was gained into the 3-5 ppm broad  
185 signal, its empirical assignment to  $\mu_3$ -OH is strongly questioned. Indeed, for the hydration  
186 degree of our samples, only two  $\mu_3$ -OH were found in the models of interest (one for (110)  
187  $12.0 \text{ OH/nm}^2$  and other for edge  $6\text{H}_2\text{O}$ ) and both are hydrogen bond donors with  $\delta > 5$  ppm  
188 (7.9 and 14.2 ppm, respectively). Moreover,  $\mu_1$ -OH and  $\mu_2$ -OH species acting as hydrogen  
189 bond donors are also impacting the 3-5 ppm broad signal. Lastly, broad signals with  $\delta > 5$   
190 ppm are thought to correspond to hydroxyls involved in the hydrogen bond network of the  
191 surfaces as hydrogen bond donors.

192 With this improved assignment, it is now possible to rationalize the impact the alumina nano-  
193 crystallite morphology on the  $^1\text{H}$  NMR spectra. As mentioned above, P-egg crystallites are  
194 rounded and smaller than those of T-flat, which are more parallelepipedic. Thus, P-egg  
195 presents a higher edge to surface ratio than T-flat, which explains the relative intensities of the  
196  $\approx 0$  ppm peaks of edge  $\mu_1$ -OH: 12% and 4% of  $^1\text{H}$  signal intensity for P-egg and T-flat  
197 respectively (Table S2). In the 1-3 ppm region, the  $\delta$  value of the most intense peak depends

198 on the sample which is a strong indication of different proportions of exposed surface types  
199 for each alumina. Indeed, the electron diffraction analysis (Figure S4) suggests that the (111)  
200 termination is more exposed in T-flat crystallites than in P-egg's. Finally, the large signal for  
201  $\delta > 3$  ppm is more intense for T-flat, which is explained by a H-bond network between  
202 hydroxyls that is more developed on the extended surface planes of T-flat than on P-egg.

203 To get further insights into the surface structure of P-egg and T-flat, the reactivity of the  
204 alumina hydroxyls were probed with chlorine. Chlorinated aluminas are used in many  
205 catalytic processes[38] but Cl can also be used as a probe for  $\mu_1$ -OH.[12,14,39] Chlorinated  
206 samples were prepared so as to have 0.5 and 1.4%<sub>w/w</sub>Cl deposited on each alumina (referred  
207 as P-egg-x%Cl and T-flat-x%Cl with x=0.5, 1.4). The effect of chlorine on the <sup>1</sup>H NMR  
208 spectra is clearly different for both aluminas (Figure 1 d and Figure S6). For P-egg, the 0 ppm  
209 signal disappears completely, as previously reported,[12,14] while the rest of the spectrum  
210 remains unchanged. For T-flat, not only does the 0 ppm signal not disappear completely, but  
211 it is also observed an intensity increase in the 3-5 ppm region, associated to an intensity  
212 decrease for  $\delta > 5$  ppm (Table S2).

213 According to the DFT OH/Cl exchange energies (S.I. S2.5, Figure 2 c), the edge  $\mu_1$ -OH sites  
214 are predominantly exchanged with chlorine out of all the considered hydroxyls. The  
215 subsequent exchanged hydroxyls would be the  $\mu_1$ -OH of the (110) surface and after that only  
216 the  $\mu_1$ -OH and  $\mu_2$ -OH sites of the (111) surface. Since the  $\approx 0$  ppm peak completely disappears  
217 for P-egg, and no impact is observed on the remaining parts of the spectrum, it is believed that  
218 only the  $\mu_1$ -OH located on the edges are exchanged with chlorine at 1.4%Cl and not those of  
219 the surfaces. For T-flat, since the peak at  $\approx 0$  ppm does not fully disappear while the 3-5 ppm  
220 and  $\delta > 5$  ppm regions are perturbed, not only the edge  $\mu_1$ -OH are exchanged but also surface  
221 hydroxyls (most likely on the (110)), disturbing the H-bond network. The signal remaining at  
222  $\approx 0$  ppm after chlorination should correspond to the (111) surface  $\mu_1$  and  $\mu_2$  hydroxyls. Just as

223 the electron diffraction analysis, the NMR results also suggest that the (111) surface is  
224 relatively more exposed in T-flat crystallites than in P-egg's. This implies that the number of  
225 edge  $\mu_1$ -OH of T-flat is not sufficient to exchange 1.4% Cl while it is the case on P-egg.

226

#### 227 **4. Conclusion**

228 The construction of the first DFT model of  $\gamma$ -Al<sub>2</sub>O<sub>3</sub> crystallite (110)-(100) edge has allowed a  
229 refined <sup>1</sup>H NMR peak assignment. It was found that the sharp peak at 0 ppm corresponds  
230 mostly to  $\mu_1$ -OH located on the edges of the crystallites that are isolated and free from  
231 hydrogen bonding. These hydroxyls are also the most favourably exchanged with chlorine,  
232 which can be considered as a selective probe of alumina edges. Overcoming the simple  
233 empirical assignment, the 1-3 ppm region corresponds to signals from not only  $\mu_2$ -OH but  
234 also from  $\mu_1$ -OH located either on the surfaces or on the edge, and that are either H-bond  
235 acceptors or free hydroxyls. Moreover, hydroxyls that are hydrogen bond donors are abundant  
236 on the surfaces and contribute to the high chemical shift broad signals. Hopefully, this novel  
237 alumina edge model and the improved assignment open new perspectives to further explore  
238 the potential of the edge sites present in industrially relevant high surface alumina crystallites.

239

#### 240 **Acknowledgements**

241 A.T.F.B. thanks A.-L. Taleb for her collaboration in HR-TEM analysis and E. Rosati, C.  
242 Guegan and C. Mancina for their contribution to sample preparation. M. Marsman (University  
243 of Vienna) is acknowledged for advice with respect to chemical shift calculations, and K.  
244 Larmier for preliminary computational investigations. Calculations were performed using  
245 HPC resources from GENCI-CINES (Grant A0020806134) and from IFP Energies nouvelles.  
246 TGIR RMN THC (FR3050 CNRS) is acknowledged for the NMR characterizations.

247 This work was funded by IFPEN and financial support from Equipex contract ANR-10-  
248 EQPX-47-01 is acknowledged. This work was supported by the LCR "CARactérisation des  
249 Matériaux pour l'Energie" (CARMEN), IFPEN/CNRS/UCBL/ENS  
250 Lyon/UNISTRA/Sorbonne Université, and is part of the "RatiOnAl Design for CATalysis"  
251 (ROAD4CAT) industrial chair, project IDEXLYON funded by the French National Research  
252 Agency (ANR-16-IDEX-0005).

## 253 **References**

- 254 [1] P. Euzen, P. Raybaud, X. Krokidis, H. Toulhoat, J.-L. Le Loarer, J.-P. Jolivet, C.  
255 Froidefond, in: F. Schuth, K. S. W. Sing, J. Weitkamp (Eds.), Handbook of Porous  
256 Solids, Wiley-VCH Verlag GmbH, Weinheim, Germany, 2002, p. 1591.
- 257 [2] H. Knözinger, P. Ratnasamy, Catal. Rev. - SCI. Eng. 17 (1978) 31.
- 258 [3] G. Busca, V. Lorenzelli, G. Ramis, R.J. Willey, Langmuir 9 (1993) 1492.
- 259 [4] M. Digne, P. Sautet, P. Raybaud, P. Euzen, H. Toulhoat, J. Catal. 211 (2002) 1.
- 260 [5] M. Digne, P. Sautet, P. Raybaud, P. Euzen, H. Toulhoat, J. Catal. 226 (2004) 54.
- 261 [6] J.H. Kwak, J. Hu, D. Mei, C.-W. Yi, D.H. Kim, C.H.F. Peden, L.F. Allard, J. Szanyi,  
262 Science 325 (2009) 1670.
- 263 [7] R. Wischert, C. Copéret, F. Delbecq, P. Sautet, Angew. Chem. Int. Ed. 50 (2011) 3202.
- 264 [8] G. Busca, Catal. Today 226 (2014) 2.
- 265 [9] M. Lagauche, K. Larmier, E. Jolimaitre, K. Barthelet, C. Chizallet, L. Favergeon, M.  
266 Pijolat, J. Phys. Chem. C 121 (2017) 16770.
- 267 [10] C. Morterra, G. Magnacca, Catal. Today 27 (1996) 497.
- 268 [11] A. Zecchina, E. Escalona Platero, C. Otero Arean, Inorg. Chem. 27 (1988) 102.
- 269 [12] A. Kytokivi, M. Lindblad, J. Chem. Soc. Faraday Trans. 91 (1995) 941.
- 270 [13] E. C. DeCanio, J. C. Edwards, J. W. Bruno, J. Catal. 148 (1994) 76.
- 271 [14] J. Hietala, A. Root, P. Knuutila, J. Catal. 150 (1994) 46.

- 272 [15] M. Taoufik, K.C. Szeto, N. Merle, I. Del Rosal, L. Maron, J. Trebosc, G. Tricot, R.M.  
273 Gauvin, L. Delevoye, Chem. Eur. J. 20 (2014) 4038.
- 274 [16] M. Delgado, F. Delbecq, C.C. Santini, F. Lefebvre, S. Norsic, P. Putaj, P. Sautet, J.-M.  
275 Basset, J. Phys. Chem. C 116 (2012) 834.
- 276 [17] P. Nortier, P. Fourre, A.M. Saad, O. Saur, J.C. Lavalley, Appl. Catal. 61 (1990) 141.
- 277 [18] M. Mavrikakis, P. Stoltze, J.K. Nørskov, Catal. Lett. 64 (2000) 101.
- 278 [19] D.W. Blakely, G.A. Somorjai, J. Catal. 42 (1976) 181.
- 279 [20] G. A. Somorjai, D. W. Blakely, Nature 258 (1975) 580.
- 280 [21] R.A. van Santen, M. Neurock, S.G. Shetty, Chem. Rev. 110 (2010) 2005.
- 281 [22] Guido Busca, Progress in Materials Science 104 (2019) 215.
- 282 [23] M.R. Bendall, D.T. Pegg, Magn. Reson. Med. 2 (1985) 91.
- 283 [24] D.G Cory, W.M Ritchey, J. Magn. Reson. 80 (1988) 128.
- 284 [25] M Robin Bendall, Roy E Gordon, J. Magn. Reson. 53 (1983) 365.
- 285 [26] D. Massiot, F. Fayon, M. Capron, I. King, S. Le Calvé, B. Alonso, J.-O. Durand, B.  
286 Bujoli, Z. Gan, G. Hoatson, Magn. Reson. Chem. 40 (2002) 70.
- 287 [27] C.J. Pickard, F. Mauri, Phys. Rev. B 63 (2001) 245101.
- 288 [28] J.R. Yates, C.J. Pickard, F. Mauri, Phys. Rev. B 76 (2007) 24401.
- 289 [29] J.P. Perdew, K. Burke, M. Ernzerhof, Phys. Rev. Lett. 77 (1996) 3865.
- 290 [30] S.N. Steinmann, C. Corminboeuf, J. Chem. Theory Comput. 7 (2011) 3567.
- 291 [31] G. Kresse, D. Joubert, Phys. Rev. B 59 (1999) 1758.
- 292 [32] G. Kresse, J. Hafner, Phys. Rev. B 49 (1994) 14251.
- 293 [33] G. Kresse, J. Furthmüller, Comp. Mater. Sci. 6 (1996) 15.
- 294 [34] M. Hunger, Catal. Rev. - SCI. Eng. 39 (1997) 345.
- 295 [35] V. M. Gun'ko, V. V. Turov, Langmuir 15 (1999) 6405.

- 296 [36] C. Chizallet, G. Costentin, H. Lauron-Pernot, M. Che, C. Bonhomme, J. Maquet, F.  
297 Delbecq, P. Sautet, *J. Phys. Chem. C* 111 (2007) 18279.
- 298 [37] X. Krokidis, P. Raybaud, A.-E. Gobichon, B. Rebours, P. Euzen, H. Toulhoat, *J. Phys.*  
299 *Chem. B* 105 (2001) 5121.
- 300 [38] C. Marcilly, in: C. Marcilly (Ed.), *Acido-basic catalysis: Application to refining and*  
301 *petrochemistry*, Editions Technip, Paris, 2006, p. 101.
- 302 [39] M. Digne, P. Raybaud, P. Sautet, D. Guillaume, H. Toulhoat, *J. Amer. Chem. Soc.* 130  
303 (2008) 11030.